Effective intermittency and cross correlations in the standard map

G. Datseris and F. K. Diakonos*
Department of Physics, University of Athens, GR-15771 Athens, Greece

P. Schmelcher†
Zentrum für Optische Quantentechnologien, Universität Hamburg, Luruper Chaussee 149, 22761 Hamburg, Germany
and The Hamburg Centre for Ultrafast Imaging, Universität Hamburg, Luruper Chaussee 149, 22761 Hamburg, Germany
(Received 16 April 2015; published 21 July 2015)

We define auto- and cross-correlation functions capable of capturing dynamical characteristics induced by local phase-space structures in a general dynamical system. These correlation functions are calculated in the standard map for a range of values of the nonlinearity parameter k. Using a model of noninteracting particles, each evolving according to the same standard map dynamics and located initially at specific phase-space regions, we show that for $0.6 < k \leqslant 1.2$ long-range cross correlations emerge. They occur as an ensemble property of particle trajectories by an appropriate choice of the phase-space cells used in the statistical averaging. In this region of k values the single-particle phase space is either dominated by local chaos ($k \leqslant k_c$ with $k_c \approx 0.97$) or it is characterized by the transition from local to global chaos ($k_c < k \leqslant 1.2$). Introducing suitable symbolic dynamics we demonstrate that the emergence of long-range cross correlations can be attributed to the existence of an effective intermittent dynamics in specific regions of the phase space. Our findings support the recently established relation of intermittent dynamics and cross correlations [F. K. Diakonos, A. K. Karlis, and P. Schmelcher, Europhys. Lett. **105**, 26004 (2014)] in simple one-dimensional intermittent maps, suggesting its validity also for two-dimensional Hamiltonian maps.

DOI: 10.1103/PhysRevE.92.012914 PACS number(s): 05.45.Ac, 05.45.Pq

I. INTRODUCTION

Dynamical systems with mixed phase space (PS) [1] are characterized by the coexistence of time scales that may differ by several orders of magnitude. The fast propagation in the chaotic sea is usually interrupted by long-time stickiness on local PS structures such as dynamical traps of hierarchically arranged islands, net traps, or dynamical traps of stochastic layers [2]. Usually the dynamics in these regions is almost regular in contrast to the stochastic profile of the complete trajectory. Furthermore, the PS geometry in the regions where regular and chaotic trajectories approach each other arbitrarily close is typically fractal and this leads to the presence of unusual statistical properties in the ensemble of the chaotic trajectories [3]. This is mainly due to the fact that the dynamics is in this case pseudoergodic [4], making impractical the use of trajectory-based common tools, such as, for example, the Lyapunov exponents or the correlation functions. In the context of Lyapunov exponents, the main interest for a nonhyperbolic Hamiltonian system is to capture the large variation of the local instability due to the coexistence of chaotic and laminar phases along a reference chaotic trajectory [5]. Suitable tools for this purpose are provided by the finite-time Lyapunov exponents [6] and the recently introduced finite-time rotation numbers [7], which turn out to be much more sensitive to local PS structures than the corresponding global quantities, thereby allowing for a better understanding of the mixed PS dynamics. This is clearly demonstrated in Ref. [8], showing that in Chirikov's standard map (SM) [9], which is a prototype Hamiltonian system with mixed phase space, the statistical distribution of the finite-time Lyapunov exponents detects stickiness in the form of a secondary peak. The SM is in general a very useful laboratory for the exploration of local PS structures being at the same time an approximate description of several physical systems, such as the kicked rotor [10], the relativistic cyclotron [11], and the equilibrium configurations of the Frenkel-Kontorova model [12]. Simple to simulate, two-dimensional, and discrete in time, the SM has been extensively studied in recent decades with emphasis on diverse dynamical aspects such as anomalous diffusion and stickiness [13], accelerator modes [14], and generating phase space partitions [15], which are closely related to the presence of local PS structures and their impact on mixed PS dynamics.

Concerning correlation functions, the investigations in area-preserving maps with mixed PS have a long history. In Ref. [16] the properly normalized relative frequency for the occurrence of a pair of PS cells separated by m iterations (a coarse grained version of the correlation function) was calculated for an ensemble of SM chaotic trajectories using a large value for the nonlinearity parameter k. An exponential decay of this quantity as a function of the delay time m was found. In Ref. [17] it was observed that by changing the value of k in the SM, the correlation functions exhibit different asymptotic behavior ranging from faster than exponential to algebraic decay. In Ref. [18] it was shown that this exponential decay of correlations is related to the dynamics in "island-free" chaotic regions and becomes a power-law decay when the chaotic trajectories evolve in a PS region possessing stability islands. Later it was recognized that the long tails in statistical distributions of area-preserving maps with mixed PS originates from stickiness effects initiating a series of works on the impact of stickiness in the dynamics and the emergence of long-range autocorrelations [11,19–25].

*fdiakono@phys.uoa.gr
†pschmelc@physnet.uni-hamburg.de

The implications of pseudoergodicity on the behavior of correlation functions are quite intricate, since these quantities contain an additional time scale (the delay time), which implies a lower cutoff on the trajectory lengths used in the corresponding time-averaging. In fact, for the correlation function to be representative for the PS dynamics it is required that the associated trajectory length is order(s) of magnitude larger than the maximum delay time. Thus, the locality of the PS structures and the conditions of long-time propagation are compelling factors, making the use of correlation functions for exploring local PS dynamics a difficult task. On the other hand, in a class of Hamiltonian systems with PS dominated by stratification due to the presence of invariant KAM spanning curves, different PS regions may be dynamically disconnected. Thus, ergodicity may be partially restored within an isolated PS region and the definition of correlation functions within such a region is plausible. Usually, in this case, even after the destruction of the invariant spanning curves, remnants of the stratified structure survive in the form of a dense set of stability islands [26]. Consequently, the stickiness on this net of dynamical traps induces large differences between the time-scale characteristic for an ergodic covering of a single PS zone through a chaotic trajectory and the time scale needed to cross the destroyed spanning curve and enter in the accessible neighboring PS zone. One could naturally think that even in this case, despite the presence of global chaos, the definition of appropriate correlation functions sensitive to the local PS structures may be possible.

The aim of the present paper is twofold. First, we introduce a class of correlation functions possessing the ability to explore the dynamics in restricted PS regions for an arbitrary Hamiltonian system. Second, using these correlation functions we analyze the dynamics of the SM close to the transition from local to global chaos. In particular, we focus on cross-correlation functions between trajectories with different initial conditions. Such a trajectory ensemble corresponds to a set of noninteracting particles each evolving according to the SM dynamics with the same k, similarly to the scheme used in Ref. [27] to study the emergence of stochasticity due to fixed-point transitions. We show that around the local-to-global chaos transition point, long-range cross correlations develop, and subsequently, inspecting the trajectories in the ensemble used for the calculation of the cross-correlation function, we reveal the presence of effective intermittency in a symbolic representation of the associated dynamics. The observed intermittency is strong in the sense that the mean waiting time in the laminar region diverges. Thus, our analysis demonstrates that the previously recorded emergence of cross correlations in a system of noninteracting particles following non-Hamiltonian 1D intermittent dynamics [28] is present also in a 2D Hamiltonian system like the SM close to the transition from local to global chaos.

Our paper is organized as follows. In Sec. II we give the definitions of the correlation functions and we introduce the dynamical system we are considering in the subsequent analysis. Section III provides the numerical results of the correlation functions in the considered model for a dense set of values of the nonlinearity parameter k around the critical value k_c, signaling the transition from local to global chaos. In Sec. IV we analyze the obtained results by performing a detailed evaluation of the characteristic trajectories and introducing an appropriate symbolic dynamics to reveal the underlying effective intermittency. Finally, Sec. V provides our concluding remarks.

II. CORRELATIONS IN THE STANDARD MAP MODEL AND BASIC OBSERVABLES

The model we consider consists of M noninteracting particles, each evolving according to the dynamics of the standard map ([9]):

$$\begin{aligned} p_{n+1}^{(i)} &= p_n^{(i)} + k^{(i)} \sin\theta_n^{(i)}, \\ \theta_{n+1}^{(i)} &= \theta_n^{(i)} + p_{n+1}^{(i)}, \end{aligned} \tag{1}$$

where $k^{(i)}$ is the control parameter of the nonlinearity and $i = 1,2,...,M$. We will here consider exclusively the case $k^{(1)} = k^{(2)} = ...k^{(M)} = k$, which simplifies the description significantly, reducing the study of the M-particle system to the study of an ensemble of initial conditions for a single particle. In this case the particle index (i) can be omitted in the description. Then the variables of the system, θ_n and p_n, stand for the single-particle angular position and momentum at time instant n, respectively, both calculated with modulo 2π. We restrict our analysis to the range $k \in [0,2]$. The system undergoes a transition from local to global chaos at the critical value $k_c = 0.971635...$ [29]. At k_c the last KAM curve with ratio ϕ (golden ratio) is destroyed and therefore chaotic orbits are not trapped between KAM tori any more, but they evolve across their remnants covering in principle all the available PS except the remaining islands of stability. Dynamically the trace of the destroyed regular PS structure is revealed in the stickiness of the chaotic orbits around these stability islands. As mentioned in the introduction, it is likely to assume that the sticky evolution of the chaotic orbits in the immediate neighborhood of the remaining stability islands may introduce some correlations even between chaotic orbits originating from different initial conditions. To explore this scenario we will calculate the autocorrelation (AC) and cross-correlation (CC) functions of the considered system for the aforementioned k values, focusing mainly on the k region, where the transition from local to global chaos takes place.

For this task one usually employs the standard definition [1] for the correlation functions:

$$\begin{aligned} \rho_{x,ij}(m) = \lim_{N\to\infty} \Bigg[& \frac{1}{N-m} \sum_{n=0}^{N-m-1} x_i(n) x_j(n+m) \\ & - \frac{1}{(N-m)^2} \sum_{n=0}^{N-m-1} x_i(n) \sum_{n=0}^{N-m-1} x_j(n+m) \Bigg], \end{aligned} \tag{2}$$

where N is the orbit's length, x represents the PS variables θ or p, m stands for the usual time-delay occurring in the correlation functions (CFs), and i, j label the different sets of initial conditions (θ_0, p_0) that define the orbits i and j. The diagonal entries $i = j$ in Eq. (2) determine the AC function, which expresses the statistical similarity of a single trajectory at any two time instances differing by m. The CC function is obtained from the nondiagonal entries $i \neq j$ in Eq. (2) and expresses the respective statistical similarity

between two different orbits (i.e., two orbits with different initial conditions) at any two time instances differing by m. The limit $N \to \infty$ is usually replaced by averaging over the entire PS requiring the system to be strongly ergodic, which is not for all the considered values of k the case for the SM. In fact, in the most interesting region of $k \in [0.6,2.0]$, the PS is mixed. As a result the associated averaging contains qualitatively different dynamical components (chaotic, regular trajectories) and washes out properties (i.e., correlations), which characterize each dynamical component separately. Thus, it is obvious that global averaging is not representative of the local structures of the phase space.

Another property that disfavors the use of the global averaging is related to the symmetries of the SM. The PS of the standard map is point symmetric around (π,π), causing the fact that for each trajectory, denoted as (θ,p), there exists a partner trajectory $(\theta,p)_{\rm ps} = (2\pi-\theta,2\pi-p)$ [where the index ps is used to notice the point-symmetric partner of (θ,p)]. This implies that the contribution to the CC function of a pair of orbits $\{a,b\}$ and the contribution of the pair $\{a,b_{\rm ps}\}$, with $b_{\rm ps}$ the point-symmetric partner of b, will be exactly opposite canceling out in the averaging. Thus, as long as there coexist orbits in the ensemble with their point-symmetric counterparts, the averaging will always lead to vanishing cross correlations.

In order to overcome both, the peculiarities of the averaging procedure originating from the fact that the ergodicity is not strongly satisfied, as well as the trivial behavior of the correlation functions due to the PS antisymmetry, we introduce here a new class of correlation functions, the localized finite-time correlation functions (LFTCFs). Their aim is to extract information on the possible emergence of correlations due to the local structures in the phase space and they are defined as follows:

$$A_x^{(d)}(m) = \lim_{S_d\to\infty}\frac{1}{S_d}\sum_{i\in\mathfrak{C}^{(d)}}\rho_{x,ii}^{(d)}(m); \qquad C_x^{(d)}(m)$$

$$= \lim_{S_d\to\infty}\frac{1}{S_d}\sum_{\substack{i,j\in\mathfrak{C}^{(d)}\\ i\neq j}}\rho_{x,ij}^{(d)}(m) \tag{3}$$

with

$$\rho_{x,ij}^{(d)}(m) = \frac{1}{N-m}\sum_{n=0}^{N-m-1} x_i^{(d)}(n)x_j^{(d)}(n+m) - \frac{1}{(N-m)^2}\sum_{n=0}^{N-m-1} x_i^{(d)}(n)\sum_{n=0}^{N-m-1} x_j^{(d)}(n+m), \tag{4}$$

where $\{x_i^{(d)}(0),x_j^{(d)}(0)\} \in \mathfrak{C}^{(d)} \subseteq PS; \quad x=\theta$ or p.

The LFTCFs in Eq. (3) are obtained by the usual definition of CFs [Eq. (2)], by fixing the trajectory length N in the ensemble to a finite value and averaging over different CFs, each calculated using trajectory pairs with initial conditions within a specific PS cell $\mathfrak{C}^{(d)}$. Local, finite-time autocorrelation (cross-correlation) functions are denoted by $A_x^{(d)}$ [$C_x^{(d)}$], respectively. The appropriate choice of N is related to the PS structure and it will be discussed in detail in the next section. The index d is used to indicate the PS domain where the cell $\mathfrak{C}^{(d)}$ belongs (see below). With S_d we notice the total number of pairs of initial conditions used for the calculation of the CFs. In Eq. (3), $\mathfrak{C}^{(d)}$ should necessarily belong only to one of the two distinguishable domains covering the entire PS:

The *chaotic domain* ($d=c$), which contains all the PS areas where local or global chaos is present. For $k \geqslant k_c$, the chaotic domain spans over the whole PS, excluding the stability islands.

The *regular domain* ($d=r$), which contains all the areas of the PS that are either stability islands or spanning curves (periodic or quasiperiodic orbits).

As an example, in Fig. 1 we show the PS of the SM for $k=0.95$. The chaotic domain corresponds to the colored regions while the regular domain to the black ones.

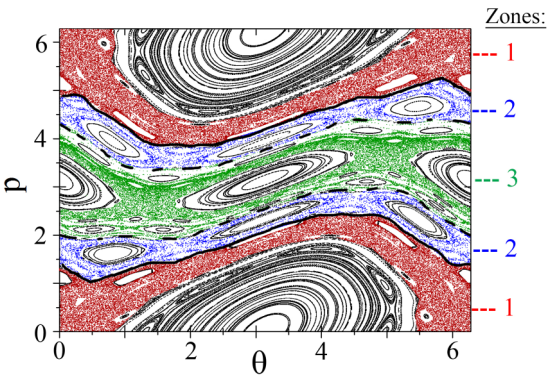

FIG. 1. (Color online) The mixed PS of the SM for $k=0.95$. The colored (gray) regions correspond to chaotic while the black regions to regular dynamics. The lines indicate the locations of Γ (dashed) and Ω (solid) invariant spanning curves. The red colored region defines zone 1, as indexed by the numbers in the column at the right-hand side of the plot, while the blue and the green colored regions define zones 2 and 3, respectively (see discussion in Sec. III).

Since the definition of the LFTCFs requires the averaging over initial conditions in a specific PS-cell, one can naturally ask about the dependence of the form of these CFs on the specific location or size of the cell within a domain as well as the length of the involved trajectories. This will be thoroughly discussed in Sec. III. Obviously the LFTCFs allow us to analyze the correlations in each dynamical component (chaotic, regular) separately, taking also into account the impact of the local PS structure. However, the cell choice requires some care since one has to ensure that it belongs entirely only to one of the two aforementioned domains.

III. NUMERICAL SIMULATIONS

For finite S_d, Eq. (3) provides us with an estimate of the LFTCFs with initial conditions in the cell $\mathfrak{C}^{(d)}$. Of course the result will in general depend on both the finite-time interval N and the position of the cell $\mathfrak{C}^{(d)}$. For a regular domain ($d=r$) the dominant frequencies define a characteristic time scale and N can be chosen to be a multiple of the period corresponding to the largest frequency peak in the related power spectrum. In addition the regular motion does not generate diffusion and therefore the evolution of the initial cell $\mathfrak{C}^{(r)}$ remains localized in PS. Thus the validity of the terms "*finite time*" and "*local*" used in Eq. (3) is straightforward for an ensemble of trajectories with initial conditions in a regular cell.

In contrary, the validity of these terms is less clear when the cell of initial conditions lies within a chaotic domain ($d = c$). To illuminate this issue we explore in more detail the PS structure. For $0.55 < k < 0.85$ local chaos appears in the vicinity of the large regular island centered around $(\pi,0)$. For $k \in [0.85,1.2]$ the PS is naturally divided into three zones, which in practice are dynamically disconnected due to the presence of invariant KAM spanning curves or their remnants. In Fig. 1 we show these zones colored red (zone 1), blue (zone 2), and green (zone 3) for $k = 0.95$. Let Γ be the last KAM spanning curve and its point-symmetric partner separating zones 1 and 2 (dashed lines in Fig. 1) and Ω the last spanning curve and its point symmetric partner separating zones 2 and 3 (solid lines in Fig. 1). Ω is the golden ratio KAM curve. At $k \approx 0.9164$ the Γ and at $k = k_c$ the Ω KAM curves are destroyed. For $k \lesssim 0.91$ the term "local" for the LFTCFs refers to dynamics within a single zone while the "finite time" is irrelevant since an ensemble of chaotic trajectories with initial conditions within a zone remains there for very large time scales ($\sim 10^8$ iterations). Although the chaotic component of the PS becomes connected through the breaking of the spanning curves, there is always strong stickiness on the boundaries, and, as a result, the mean time needed for a trajectory starting within each one of these zones to enter in a neighboring zone is very large ($\sim 10^4$–10^8 iterations). In fact, even at $k = 1$ where all spanning curves are broken, a trajectory starting in the red zone needs at least 10^3 iterations to enter in the blue zone, while a trajectory starting in the blue zone needs at least $\sim 10^5$ iterations to enter into the green zone. To illustrate this in a more transparent way, we calculate the cumulative distribution function $F_T(t) := \text{Prob}(T \leqslant t)$ of the first passage time T for a chaotic trajectory to cross up to time t, either the remnants of Γ starting from zone 1 or the remnants of Ω starting from zone 2. In practice, to find $F_T(t)$ we start with an ensemble of 10^5 trajectories in a selected zone (1 or 2) and we determine the number of trajectories having first passage time T smaller than t normalizing by the total number of trajectories in the ensemble.

In Fig. 2 we show $F_T(t)$ for the first passage time from zone 1 to zone 2 (red dashed line) as well as the first passage time from zone 2 to zone 3 (blue solid line). As expected both curves saturate at $F_T = 1$ for $t \to \infty$. We clearly observe the lower cutoff at times $t_{12,\min} \approx 10^3$ and $t_{23,\min} \approx 10^5$, respectively. In addition the corresponding mean times [defined by $F_T(\langle t \rangle) = 1/2$] are $\langle t_{12} \rangle = 2.6 \times 10^4$ and $\langle t_{23} \rangle = 2.8 \times 10^6$. Thus, as dictated by the results shown in Fig. 2, there are well-defined timescales that restrict the dynamics to a single zone. This justifies the use of the terms "finite time" and "local" in the correlation functions of Eq. (3) even for chaotic trajectories with k larger but close enough to k_c, so that the PS stratification into zones, as demonstrated in Fig. 1, is still dynamically valid. For a large ensemble of trajectories with initial conditions in the red zone, choosing, for example, $N \approx 10^4$ in Eq. (3) it is guaranteed that the obtained correlation functions characterize the local dynamics within this zone. A similar argument applies also for analogous ensembles of trajectories with initial conditions in the other two zones. The general conclusion is that LFTCFs are especially useful for the description of correlations at least in two cases: (i) when the PS of the dynamical system is stratified into zones by invariant spanning

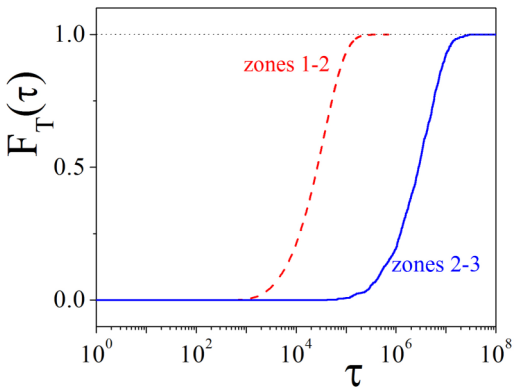

FIG. 2. (Color online) The cumulative distribution functions for the probability of a chaotic trajectory to cross up to time t the second to last spanning curve (red dashed line) starting from a PS cell in the first zone (region 1 in Fig. 1) and the last spanning curve (blue solid line) starting from a PS cell in the second zone (region 2 in Fig. 1). Both functions are calculated using $k = 1$. The dotted line at $F_T(t) = 1$ is plotted to guide the eye.

curves and within each zone local chaos is fully developed ($0.85 < k < 0.91$ for the SM) and (ii) close to the critical point for a dynamical system exhibiting a transition from local to global chaos ($0.91 < k < 1.2$ for the SM). Far beyond the critical point ($k \gg k_c$ for the SM), when the chaotic sea becomes almost homogeneous and dominating in PS while the remnants of the regular dynamics shrink significantly, the LFTCFs converge rapidly, i.e., for relatively small trajectory length N, to the usual correlation functions in Eq. (2) and become independent of the cell in the chaotic domain.

Since the delay time m should be much smaller than the length of the trajectories involved in the calculation of the LFTCFs we have to choose N as large as possible in order to allow for a large variation of m. On the other hand, for $k \gtrsim k_c$, N should be of the order of the minimum first passage time in the corresponding zone. For a given N, in order to ensure that the obtained numerical results are representative of the limit $S_d \to \infty$, we use as criterion the convergence of 2 significant digits when increasing S_d by a factor of 10. In addition the convergence with respect to the used length of the trajectories in the ensemble is tested by increasing N by a factor of 2. We found empirically that taking the values $S_d = 5 \times 10^5$ and $N = 5 \times 10^3$ in the calculation of Eq. (3) we achieve the required convergence. Thus, in the following discussion, if not stated differently, we present results using exclusively these parameter values for N and S_d.

A. Correlation functions in the regular domain

First we discuss the results for LFTCFs using initial condition cells in the regular domain, which turn out to possess some universal features. Cells within the regular domain contain quasiperiodic and periodic orbits. The corresponding LFTCFs perform oscillations around zero. Increasing S_d the amplitude of the oscillations diminishes, tending to zero for large m. This is due to the fact that the ensemble averaging is over oscillating forms with slightly shifted frequencies, which interfere destructively canceling each other. This effect

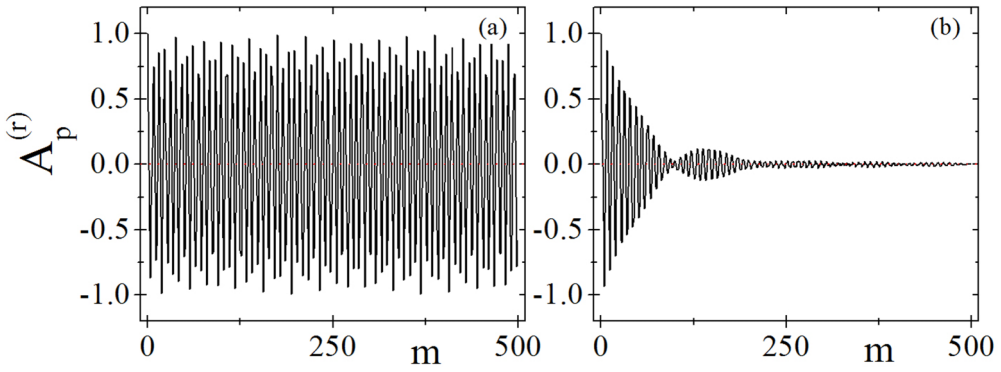

FIG. 3. (Color online) Numerical demonstration of the cancellation of the correlations in the regular domain. Shown is $A_p^{(r)}$ of orbits in a cell of size 0.5×0.5 within the stability island centered around $(\pi,0)$ when (a) a single trajectory and (b) 10^5 trajectories are used in the averaging. The $C_p^{(r)}$s (not shown) have similar form. Analogous results are obtained also for the LFTCFs of the θ variable, for all $\mathfrak{C}^{(d)}$ within the regular domain.

is demonstrated in Fig. 3, where we plot $A_p^{(r)}$ in (a) with $S_d = 1$ and in (b) with $S_d = 10^5$. The $C_p^{(r)}$ in the same cell (not shown here) converges also to an oscillatory form around zero, decaying much faster ($m \approx 30$) and having initially ($m < 30$) a very small amplitude [$O(10^{-3})$] due to different normalization.

This is a typical behavior for all cells in the regular domain. Since the LFTCFs in the regular domain oscillate always around zero we will not consider them furthermore in the following.

B. Autocorrelations in the chaotic domain

As already mentioned, the LFTCFs may depend on the specific location of the cell within the chaotic domain. We start our analysis choosing as cell $\mathfrak{C}^{(c)}$ the square [0,0.25] × [0,0.25] in the (θ, p) plane, which is in the immediate neighborhood of the first-order unstable fixed point (0,0) of the SM. We first calculate the LFTCFs in this cell and subsequently we explore their dependence on the location or the size of the cell.

In Figs. 4(a) and 4(b) we present $A_x^{(c)}$ for $k = 0.95$ using the phase space variables $x = p$ [Fig. 4(a)] and $x = \theta$ [Fig. 4(b)], respectively. Figures 4(c) and 4(d) show componentwise [p (c), θ (d)] a typical trajectory of the SM in zone 1 of the chaotic domain for this k value.

Let us first discuss the behavior of the $A_\theta^{(c)}$, which is mostly small fluctuations around zero. This is easily explained by the form of the θ time series. For the considered k values θ performs an oscillatory motion. Consequently, also the corresponding $A_\theta^{(c)}$ for a single trajectory possesses an oscillatory form. Averaging over different orbits will induce

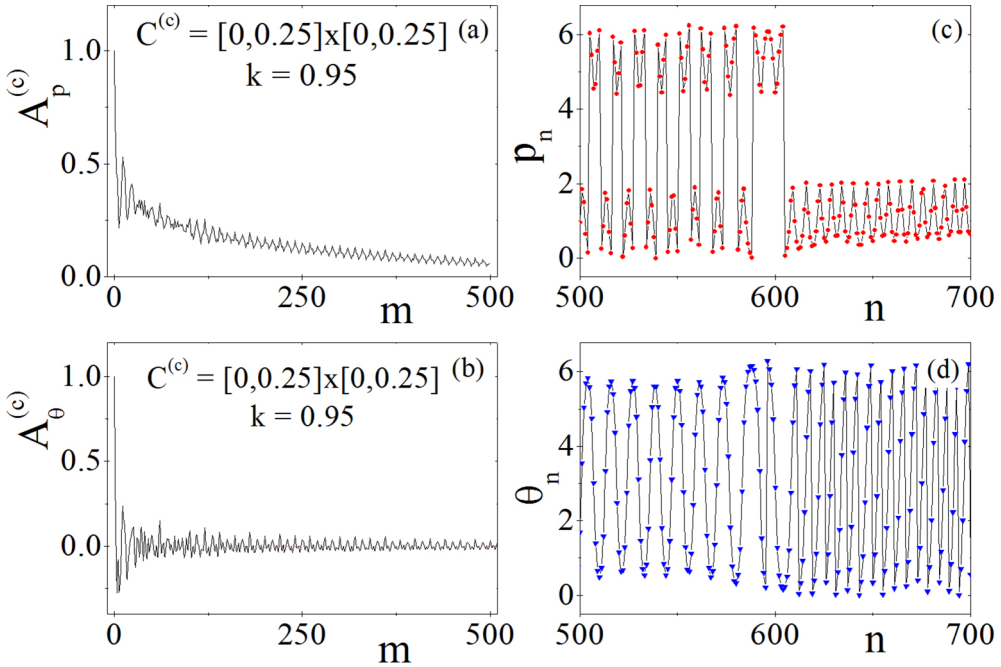

FIG. 4. (Color online) Left subfigures depict the average $A_x^{(c)}$ for the cell [0,0.25] × [0,0.25] in $x = p$ (a) and $x = \theta$ (b) variables for $k = 0.95$. Right subfigures are typical time-series for p and θ with initial conditions in this cell. Subfigure (c) corresponds to p_n and (d) to θ_n versus n (number of iterations).

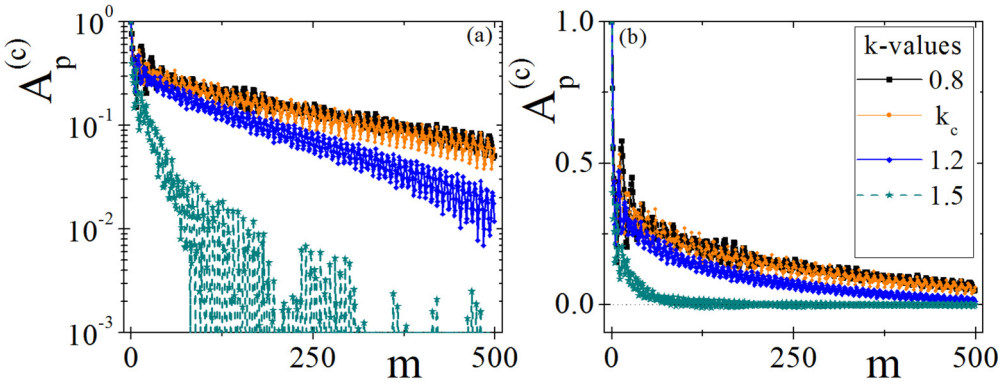

FIG. 5. (Color online) (a) $A_p^{(c)}$ in the cell $[0,0.25] \times [0,0.25]$ for a wide range of k values plotted in linear scale. An ensemble of $S_d = 5 \times 10^5$ orbits each of length $N = 5 \times 10^3$ is used. (b) The same plot in semilog scale. The $A_p^{(c)}$s are normalized to one at $m = 0$ by dividing the autocorrelation function of each trajectory in the ensemble with the corresponding standard deviation.

cancellations since the different oscillatory orbits vary in phase, amplitude, and frequency. This is actually the case for all values of k, up to $k \approx 1.5$, where the orbits become strongly chaotic characterized by irregular fluctuations, independently of the cell location in PS. Notice here that a similar behavior (fluctuations around zero) is observed for $C_\theta^{(c)}$s, and they also will not be considered furthermore in the following. Thus our subsequent analysis focuses only on the correlations of the p-component.

In contrast with the $A_\theta^{(c)}$, the autocorrelation of p, as observed in Fig. 4(a), is not trivial and the form of the corresponding trajectory [Fig. 4(c)] is qualitatively different. To explore further the autocorrelations of p we calculated $A_p^{(c)}$ for several values of the parameter k. The results are summarized in Fig. 5. In all calculations we used initial conditions in the cell $[0,0.25] \times [0,0.25]$.

In each case the convergence criteria are well satisfied. Considering the behavior in the semilog scale shown in Fig. 5(b), we observe an exponential decay trend for all values of $k \in [0.6,1.5]$. Although the exponential behavior is evident, there are fluctuations of the $A_p^{(c)}$ around the exponential envelope. These fluctuations are not of statistical origin since they persist by increasing the number of trajectories in the ensemble by a factor of 10^2. In fact, they can be attributed to the stickiness of the chaotic trajectories to the stable manifolds of the set of unstable periodic orbits surrounding the stability islands. The $A_p^{(c)}$s decay to zero significantly faster for all $k > 1.2$ reaching an almost instantaneous decay for $k \gtrsim 1.5$. The reason for this behavior will be discussed in depth in the next section where an orbit analysis is presented. Despite the oscillatory fluctuations of the $A_p^{(c)}$s it is useful to perform a fit using an exponential function,

$$f_{\mathrm{AC},p}(m) = f_0 e^{-m/\tau(k)}, \tag{5}$$

to determine the characteristic rate $\frac{1}{\tau(k)}$ for the exponential decay of the autocorrelations at different k values. The resulting $\tau(k)$ is shown as a function of k in Fig. 6.

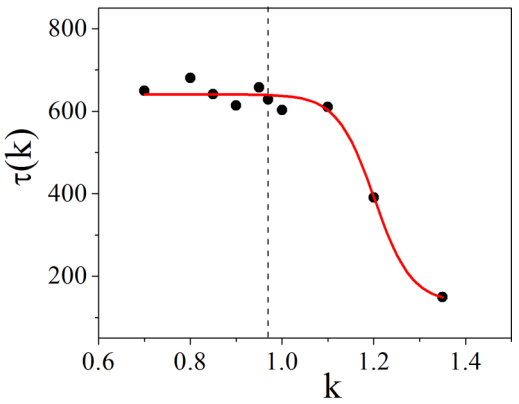

FIG. 6. (Color online) The inverse decay rates $\tau(k)$ of the $A_p^{(c)}$s (calculated using initial conditions in the PS cell $[0,0.25] \times [0,0.25]$) shown versus k (black circles). The red solid line is an interpolating sigmoidal curve to guide the eye. The vertical dotted line indicates the location $k = k_c$.

For $k \in [0.6,k_c]$ where local chaos is present, the decay rates reside within a characteristic plateau, possessing an approximately constant value of $\frac{1}{650}$. Above k_c where the transition from local to global chaos takes place, the decay rates rapidly increase and $\tau(k)$ approaches zero for $k \approx 1.5$. In Sec. IV we will see that the form of the chaotic trajectories changes significantly for $k > 1.5$ being characterized by irregular fluctuations, while this is not the case for $k < 1.5$. It will also become evident that the transition from local to global chaos induces this change in the orbits' structure, leading to vanishing LFTCFs for $k > 1.5$.

Let us now turn to the dependence of the $A_p^{(c)}$s on the cell's location within the chaotic domain. This is demonstrated in Fig. 7, showing $A_p^{(c)}$s calculated for different cell locations.

It is evident that the $A_p^{(c)}$s depend on the zone where $\mathfrak{C}^{(c)}$ is located. Furthermore, we have checked the dependence of these results on the location of the cell $\mathfrak{C}^{(c)}$ within each zone. We have found that the form of the $A_p^{(c)}$ does not change as we move $\mathfrak{C}^{(c)}$ within a zone, provided that we avoid the mixing of different PS domains (regular, chaotic). In addition, the $A_p^{(c)}$ form in zones 2 and 3 is very similar.

C. Cross correlations in the chaotic domain

Proceeding along the same lines as for the case of the autocorrelations, we analyze the localized finite-time cross-correlation functions using as $\mathfrak{C}^{(c)}$ the cell $[0,0.25] \times [0,0.25]$.

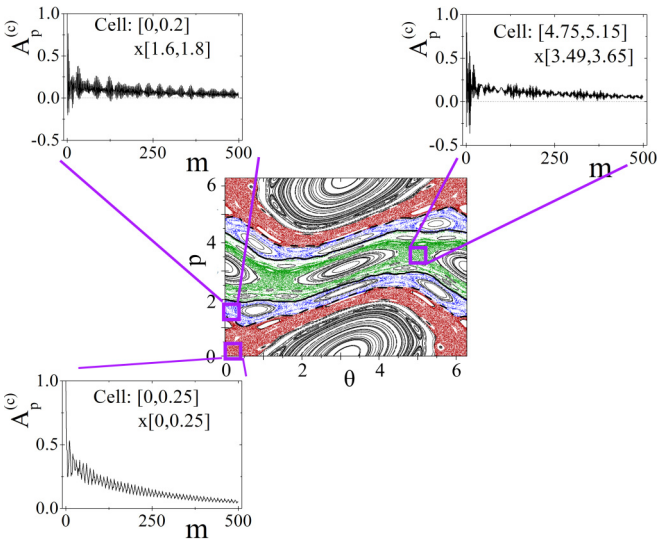

FIG. 7. (Color online) The $A_p^{(c)}$s belonging to the different zones of the chaotic domain at $k = 0.95$.

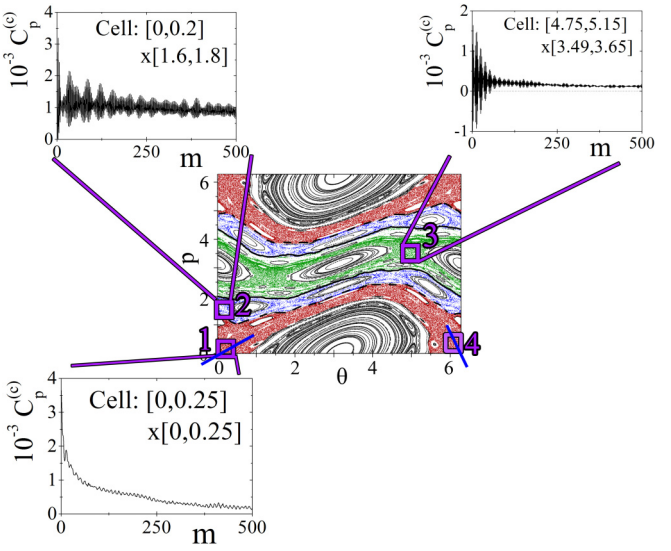

FIG. 9. (Color online) The $C_p^{(c)}$s calculated for $k = 0.95$ using PS cells located in different zones of the chaotic domain. For zone 1 we use $\mathfrak{C}^{(c)} = [0,0.25] \times [0,0.25]$, for zone 2 $\mathfrak{C}^{(c)} = [0.02,0.17] \times [1.66,1.8]$, and for zone 3 $\mathfrak{C}^{(c)} = [4.82,5.03] \times [3.57,3.68]$. Each cell is numbered with a violet-colored number. The blue lines above cells 1 and 4 correspond to the fixed point's (0,0) eigenvectors (see end of Sec. IV). The blue line above cell 1 represents the unstable eigenvector, whereas the blue line above cell 4 represents the stable eigenvector.

In Fig. 8 we present the $C_p^{(c)}$ with initial conditions in this cell for various k values.

Like in the $A_p^{(c)}$s case, the form of the $C_p^{(c)}$s varies continuously with k and for $k \gtrsim 1.5$ the $C_p^{(c)}$s approach zero rapidly with increasing m [see Fig. 8(a)]. Despite similarities, the structure of the $C_p^{(c)}$s is quite different from that of the $A_p^{(c)}$s, as it becomes evident if we inspect the $C_p^{(c)}$s in log-log [Fig. 8(b)] and log-linear [Fig. 8(c)] scales. Notice that the difference of approximately three orders of magnitude in the initial values of $C_p^{(c)}$ and $A_p^{(c)}$ relies on the fact that the cross-correlation function of each pair of orbits in the corresponding ensemble is not normalized to one at $m = 0$ in contrast to the autocorrelation functions (see caption of Fig. 8).

In Figs. 8(b) and 8(c) it is clearly seen that, neglecting small amplitude fluctuations, the $C_p^{(c)}$s show either a logarithmic or a power-law behavior, thus they possess long-range characteristics. In fact, for $k < k_c$ the $C_p^{(c)}$s can be better described as a logarithmic function of the delay m, while for $k_c < k < 1.5$ they follow approximately a power-law. Since the long-range character of the $C_p^{(c)}$ weakens as k increases beyond k_c, it is natural to ask the question whether it is related to the local structure of the chaotic domain induced by the last KAM spanning curves. Therefore, in the following we will try to explain the emergence of long-range correlations by exploring in detail the SM chaotic dynamics close to k_c. In a recent study [28], it has been shown that long-range cross correlations can emerge in systems of noninteracting particles, each performing the same intermittent dynamics. Thus, one could ask if any kind of intermittent behavior within the chaotic domain of the standard map for these k values is present (at least effectively) and generates these long-range cross correlations.

Before we address the possibility of intermittency in the SM, a study of the dependence of the form of the $C_p^{(c)}$s on the location of the cell $\mathfrak{C}^{(c)}$ is in order. Concentrating on the case $k = 0.95$ we calculate as a first step the $C_p^{(c)}$s using cells located in the different zones of the chaotic domain as presented by the different coloured regions in Fig. 1. The results of the corresponding simulations are summarized in Fig. 9.

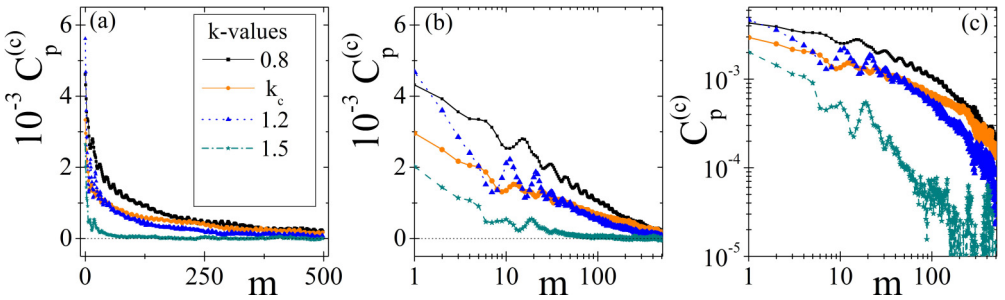

FIG. 8. (Color online) $C_p^{(c)}$ for an ensemble of 5×10^5 chaotic trajectories with initial conditions in $\mathfrak{C}^{(c)} = [0,0.25] \times [0,0.25]$ (zone 1) obtained using $k = 0.8$ (black line, squares), $k = k_c$ (orange line, circles), $k = 1.2$ (blue line, triangles) and $k = 1.5$ (green line, stars). (a) Linear-linear, (b) linear-log, and (c) log-log scale. The cross-correlation function of each pair of trajectories in the ensemble is normalized by dividing with the root of the product of the standard deviations of those trajectories.

In Fig. 9 it clearly can be seen that the $C_p^{(c)}$s in zones 2 and 3 have a quite similar form while the $C_p^{(c)}$ in zone 1 behaves differently. In the next section, this will be explained by exploring the dynamics in the neighborhood of the first-order unstable fixed point (0,0). As in the case of the $A_p^{(c)}$s, the results for $C_p^{(c)}$s within each zone do not depend on the location of the cell $\mathfrak{C}^{(c)}$. However, we observe a very slow convergence when $\mathfrak{C}^{(c)}$ is located in the position "4" within zone 1 (see Fig. 9). This strange behavior will also be discussed at the end of the next section. Notice that in the case of zone 2, since the chaotic sea is very thin, one has to use particularly small cells for the calculation of the $C_p^{(c)}$s. Due to the fact that the $C_p^{(c)}$s in zones 2 and 3 are asymptotically constant while the $C_p^{(c)}$ in zone 1 has an algebraically decaying profile, we will focus in the next section exclusively on the emergence of cross correlations in the latter zone.

IV. INTERMITTENCY AND ORBIT ANALYSIS

Intermittency is characterized by long intervals of regular motion (laminar phase) of the trajectories, interrupted by chaotic bursts [30]. At a first glance there is no connection of the Eq. (1) describing the evolution in the SM with the normal form of intermittent dynamics [1]. Therefore, it is not expected to find intermittent characteristics in the first iterate of the SM. On the other hand, an effective dynamics of the p variable could generate such a behavior possibly in higher iterates. In order to inspect this hypothesis, a more in-depth analysis of the trajectories in the parametric region $k \in [0.6,1.5]$, where the local to global chaos transition takes place, is required. Furthermore, as we have shown in the previous section, the long-range slowly decaying cross correlations that could be associated with intermittent dynamics [28] occur exclusively in SM trajectories evolving within zone 1 of the PS. Thus, in the following we will focus on dynamical characteristics of the chaotic trajectories in this PS region for $k \lesssim k_c$.

In this range of k values the p component of all trajectories in the chaotic region of zone 1 follows the behavior shown in Figs. 10(a)–10(c). For k beyond 1.5 this structure is essentially destroyed, becoming gradually a completely irregular time-series of random fluctuations. A closer look at Figs. 10(a)–10(c) reveals that the time series of p has a very intriguing structure. Considering as "down" the p values below π and as "up" the p values above it, we observe [see Figs. 10(a) and 10(b)] that the p time series consists of parts in which it is consecutively jumping up and down and parts in which it stays either only up or only down for a large number of iterations. This resembles roughly an intermittent time series where the laminar phase corresponds to intervals for which the p values are only up or only down, while the chaotic bursts correspond to intervals with successive up-down (or vice-versa) jumps of p.

Zooming in at smaller time scales [Fig. 10(c)] we observe that the p time series consists of many subintervals each containing 4 to 7 points (with p values all above or all below π) forming an almost triangular structure. This property is typical for any p time series in zone 1 of the chaotic domain and it also does not depend on the time interval we zoom into. As demonstrated in Fig. 11, it originates from the unstable fixed points of order 4, 5, 6, and 7 of the SM. These are densely embedded in zone 1 and their manifolds affect the trajectories leading to the triangular structure formation. The emergence of the latter requires the synergy of the already-mentioned unstable fixed points and a spanning curve (or its remnants) acting as a separatrix, which keeps p confined in zone 1.

To illustrate this, it is useful to consider the trace of the triangular structure in PS. Starting from the neighborhood of the PS point at (0,0) the trajectory approaches the neighborhood of the PS point $(2\pi,0)$ in 4 to 7 iterations forming the triangular structure in the p time series. After reaching $(2\pi,0)$ the trajectory either returns to the neighborhood of (0,0) in the next iteration, extending the duration of the laminar phase, or it jumps to the neighborhood of $(2\pi,2\pi)$ signaling the beginning

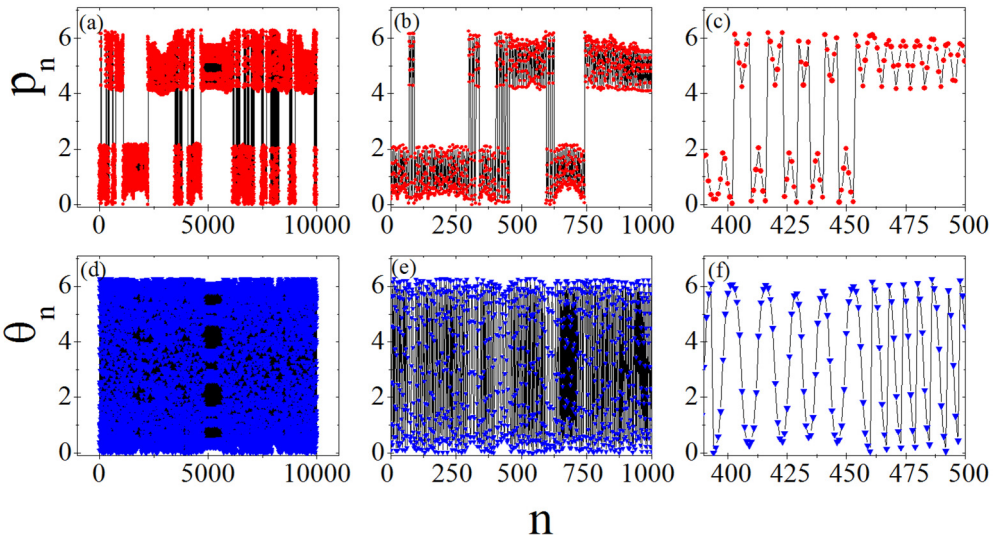

FIG. 10. (Color online) Time-series of the variables p (a, b, c) and θ (d, e, f) of the standard map, for a typical orbit within the chaotic domain, for $k = 0.95$ and initial conditions (0.1,0.2) (n is the number of iterations). Shown are (a, d) the first 10^4 iterations, (b, e) a zoom-in in the region $[0,10^3]$, and (c, f) a zoom-in in the region [400,500] of this orbit.

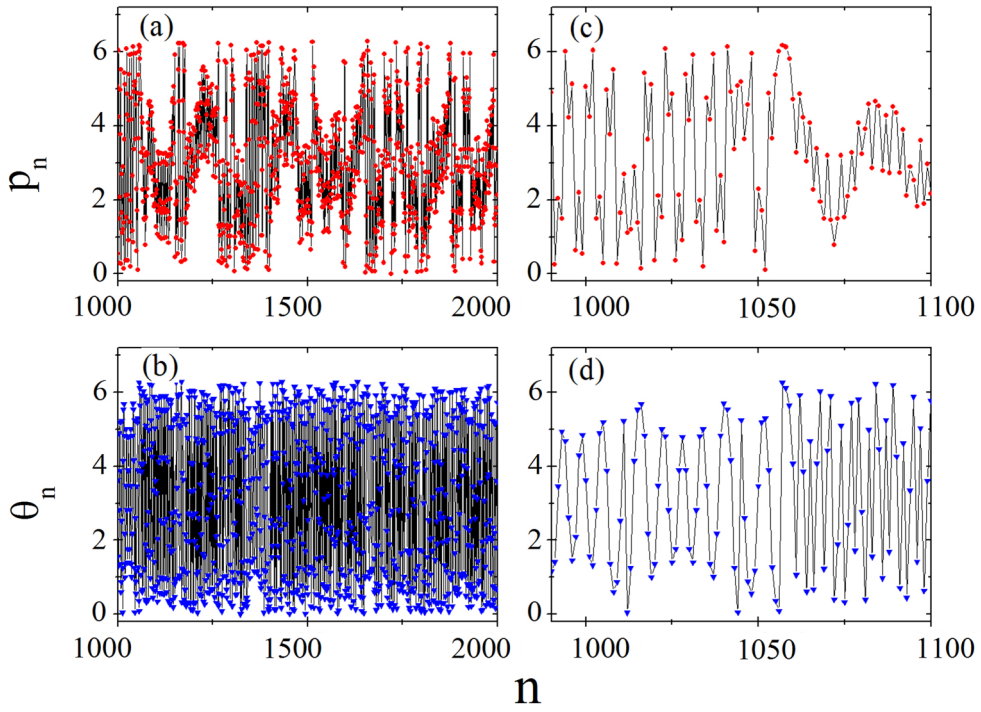

FIG. 11. (Color online) A typical trajectory [p_n shown in (a), θ_n shown in (b)] for $k = 1.8$ and initial conditions (0.2,0.1) (n counts the number of iterations). In the zoom-in of the p_n component, shown in (c), it is clearly seen that the triangular substructure in the time series of p is not sustained and a laminar phase (as defined in Sec. IV) does not exist. In (d) we also show for completeness a zoom-in of the θ_n component.

of a "chaotic burst." The same process can also take place for trajectories involving the neighborhoods of the PS points $(2\pi,2\pi)$ and $(0,2\pi)$, which are the point-symmetric partners of (0,0) and $(2\pi,0)$. During the chaotic burst interval of the p time series, the variable θ performs an oscillation from 0 to 2π and back (full cycle). When the p time series is in a laminar phase then the θ time series consists of half cycles either from 2π to 0 ("up" laminar phase of p) or from 0 to 2π ("down" laminar phase of p). This behavior is clearly displayed in Fig. 10(f).

For $k > k_c$ the last spanning curve is destroyed. Therefore, p is not bounded anymore, and the triangular structure is gradually degraded. However, for k values up to 1.5 the remnants of the separatrix still keep for long time intervals the p trajectory trapped in zone 1 and, therefore, although slightly deformed, the triangular structure is preserved. As a consequence the corresponding $C_p^{(c)}$s can exhibit long-range correlations for delay times comparable with the time scale needed for the p trajectory to escape from zone 1. For example, at $k = 1.2$ although the separatrix is destroyed, orbits with initial conditions in the neighborhood of (0,0) and length about $N = 10^4$ still exhibit the triangular structure without any significant change. However, orbits with $N = 10^6$ have escaped through the traps created by the residues of the separatrix and they follow an irregular (chaotic) motion for large time intervals. This behavior is typical for all p time series when $k > k_c$. Furthermore, the structure of a typical PS trajectory changes completely for $k > 1.5$, as shown in Fig. 12. Zooming in we observe that the time series is completely irregular in both θ and p without any structure, which could lead to a nontrivial behavior of the LFTCFs. This confirms the results presented in the previous section for k values in this range.

The previous discussion suggests representing the p time series by defining a suitable symbolic dynamics: every triangular unit consisting from 4 to 7 values of p below π is mapped to "0" and every triangular unit consisting from 4 to 7 values of p above π is mapped to "1." Obviously the opposite choice makes no difference. With this representation of the orbit we can easily define the laminar phase as a string of consecutive 1s or 0s, i.e., 11111111..., and the chaotic bursts as strings that have alternating 1s and 0s, i.e., 10101010.... Calculating the $C_p^{(c)}$s with the symbolic time series yields identical results to those in the previous section, scaled in time by a constant factor of $\approx$0.2 since every 4–7 points of the original trajectory are mapped to one point in the symbolic time-series.

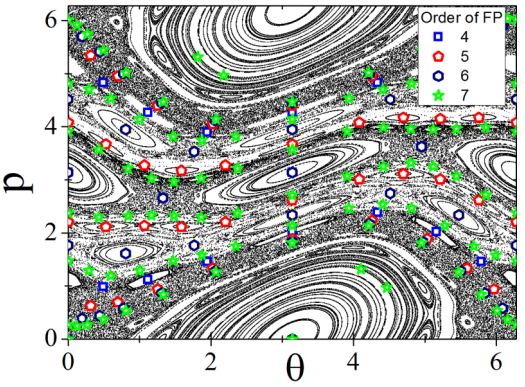

FIG. 12. (Color online) Fixed points of the standard map for $k = 1.0$ found by the method introduced in Ref. [31].

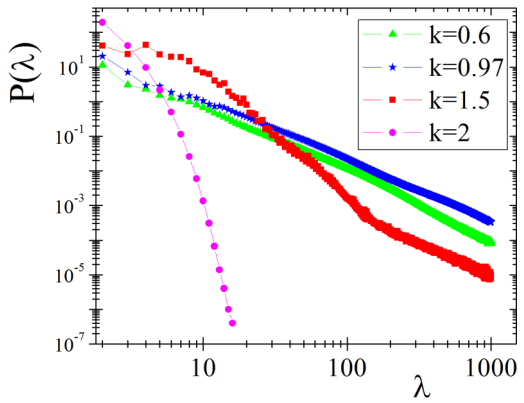

FIG. 13. (Color online) Laminar length distributions $P(\lambda)$ for various values of k, shown in log-log scale. We used 5×10^5 trajectories with initial conditions in the cell $[0,0.25] \times [0,0.25]$ and verified the independence of the cell location in zone 1.

It is now straightforward to calculate the lengths λ of the laminar phases and to obtain the laminar length distributions. We used ensembles of 5×10^5 trajectories of length $N = 1.5 \times 10^4$ with initial conditions in the cell $[0,0.25] \times [0,0.25]$, for each k value. The results are presented in Fig. 13. We checked convergence by increasing the number of trajectories in the ensemble by a factor of 10. The result coincides within three significant digits with that presented in Fig. 13. Remarkably enough it turns out that the laminar length distribution as defined above possesses some kind of universality. To verify this we recalculated this distribution by changing the size and the location of the cell of initial conditions in the chaotic domain of zone 1 and we found, for given k, the same result within a two significant digits accuracy.

The distributions shown in Fig. 13 follow approximately power laws for $k \in [0.6, k_c]$. Especially at $k = k_c$ the laminar length distribution is very close to a power law. Beyond k_c the distributions resemble a power law but this form quickly dissolves, already having deviations at $k = 1.2$. For $k > 1.5$ the laminar lengths as well as the associated symbolic dynamics lose their meaning, as the orbits no longer possesses the aforementioned triangular structure.

The fact that for k close to k_c the laminar length distributions resemble a power law is connected directly with intermittency. Such a relation is well established [1] in the literature. In Ref. [28] this property was used for a system of noninteracting particles, each obeying independently intermittent dynamics of Pomeau-Manneville type [30] in one dimension, to demonstrate the emergence of long-range (power-law) cross correlations among the particles despite the fact that they do not interact with each other. This unexpected result was explained considering a set of different trajectories with fixed length L (corresponding to trajectories of different particles) and employing a symbolic code for their representation using the symbol "0" for a trajectory point in the laminar phase and the symbol "1" for a trajectory point in the irregular (chaotic) phase. The resulting long-range cross correlations were attributed to the formation of a fractal set from all symbols "1" in the ensemble of the particle trajectories whenever the mean laminar length $\langle\lambda\rangle$ of the underlying laminar length distribution diverges. This is the case when the exponent in the laminar length distribution is in the interval $(-2, -1)$ (for exponents in $[0, -1]$ there is no normalizable laminar length distribution). Coming back to the system considered here and applying a power-law fit of the form

$$f_P(\lambda) = \beta\lambda^{\alpha} \tag{6}$$

to the laminar length distribution at $k = k_c$, we find $\alpha = -1.85$. This implies that the average laminar length is

$$\langle\lambda\rangle = \int_2^{\infty} f_P(\lambda)\lambda d\lambda = \int_2^{\infty} \lambda^{-0.85} d\lambda \to \infty, \tag{7}$$

fulfilling the requirements for the emergence of long-range cross correlations according to Ref. [28].

Two final comments are in order. As stated in Sec. III C, in the calculation of the $C_p^{(c)}$ within zone 1 we observed a very slow convergence when the cell of initial conditions $\mathfrak{C}^{(c)}$ was chosen in the neighborhood of $(2\pi,0)$ (cell with index "4" in Fig. 9). Here we will argue that this slow convergence is related to the presence of the stable manifold of the first-order fixed point in this cell. To illustrate this it is useful to derive the corresponding stable and unstable eigenvectors in terms of the nonlinearity parameter k:

$$\text{unstable}: \begin{pmatrix} \frac{-k+\sqrt{(4+k)k}}{2} \\ 1 \end{pmatrix} \quad \text{stable}: \begin{pmatrix} -1 \\ \frac{-k+\sqrt{(4+k)k}}{2} \end{pmatrix}. \tag{8}$$

For $k \approx 1$ these eigenvectors are:

$$\text{unstable}: \begin{pmatrix} 0.62 \\ 1 \end{pmatrix} \quad \text{stable}: \begin{pmatrix} -1 \\ 0.62 \end{pmatrix}. \tag{9}$$

Their direction is shown by the blue lines in Fig. 9. According to this figure the cell with index "1" contains the unstable manifold of (0,0) while the cell "4" contains the stable manifold. Although we were not able to determine the exact mechanism that induces the aforementioned slow convergence, we numerically proved that the stable manifold is the origin of this effect. To this end we calculated the $C_p^{(c)}$ for the time-reversed dynamics (which transform the stable manifold to an unstable one) of the SM:

$$\begin{aligned} \theta_{n+1} &= \theta_n - p_n, \\ p_{n+1} &= p_n - k\sin\theta_{n+1}, \end{aligned} \tag{10}$$

using initial conditions in the cell "4." The obtained $C_{L,p}^{(c)}$ turned out to be identical to that using forward in time dynamics and initial conditions in the cell "1." This clearly verifies our previous argumentation.

The last issue to be discussed concerns the understanding of the qualitatively different behavior of the $A_p^{(c)}$s and $C_p^{(c)}$s for k values around k_c. For this purpose let us consider more carefully the definition of the LFTCFs in Eq. (3). The sum $\sum_{i,j\in\mathfrak{C}^{(c)}}$ in Eq. (3) implies a summation over initial conditions i, j either with $i = j$ (autocorrelations) or with $i \neq j$ (cross correlations), where $x_i^{(c)}(0)$, $x_j^{(c)}(0)$ lie in the PS cell $\mathfrak{C}^{(c)}$. Focusing on the case $i \neq j$ and assuming that ergodicity is valid within a single PS zone, we could consider the chaotic trajectory j as equivalent to the trajectory i shifted forward in time by $n_{r,i}$ iterations, where $n_{r,i}$ is the recurrence time in $\mathfrak{C}^{(c)}$ for the trajectory i. Then we could approximately write

$x_j^{(c)}(n+m) \approx x_i^{(c)}(n+n_{r,i}+m)$ and the sum over initial conditions occurring in the definition of the $C_p^{(c)}$s could be written as

$$\sum_{i,j\in\mathfrak{C}^{(d)}} = \sum_i \sum_{n_{r,i}} p(n_{r,i}), \tag{11}$$

where $p(n_{r,i})$ is the distribution of the recurrence times in $\mathfrak{C}^{(c)}$. Thus, the averaging over different trajectory pairs is equivalent to an averaging over single trajectories like in the autocorrelation case, performing a random additional time shift following the recurrence time distribution and summing over all possible shifts. When the cell is located in the immediate neighborhood of the unstable fixed point (0,0) the distribution $p(n_{r,i})$ can be approximated by the laminar length distribution attaining a power-law form. If the cell $\mathfrak{C}^{(c)}$ is small, the distribution $p(n_{r,i})$ becomes a good approximation independent of i and one can use the notation n_r for $n_{r,i}$. Then the LFTCF in Eq. (3) can be written as

$$\begin{aligned} C_x^{(c)}(m) = \lim_{S_d\to\infty} \frac{1}{S_d} \sum_i \sum_{n_r} p(n_r) \\ \times \Bigg[\frac{1}{N-m} \sum_{n=0}^{N-m-1} x_i^{(c)}(n) x_i^{(c)}(n+n_r+m) \\ - \frac{1}{(N-m)^2} \sum_{n=0}^{N-m-1} x_i^{(c)}(n) \sum_{n=0}^{N-m-1} x_i^{(c)}(n+n_r+m) \Bigg]. \end{aligned} \tag{12}$$

The term in the brackets is the autocorrelation function for the trajectory $x_i(n)$ evaluated at the delay time $n_r + m$. As we have shown in Sec. III B the $A_p^{(c)}$s in zone 1 follow, for given k, an exponential form. The corresponding characteristic exponent $\tau(k)$ is defined as an ensemble property. Calculating the autocorrelation functions for individual trajectories forming the ensemble, we find that they can be approximated also by exponential functions of the delay m, however, with an exponent $\tau_i(k)$, which depends on the initial conditions of the trajectory i. Thus, after performing the summation over i we can approximate $C_p^{(c)}$ in zone 1 as

$$C_p^{(c)}(m) \approx \lim_{S_d\to\infty} \frac{1}{S_d} \sum_i \sum_{n_r} p(n_r) e^{-\frac{n_r+m}{\tau_i}}, \tag{13}$$

where $p(n_r) \sim n_r^{\alpha}$ with $\alpha \approx -1.85$ as dictated by the laminar length distribution. The sum over n_r can be performed leading to

$$C_p^{(c)}(m) \approx q_N \sum_i \tau_i^{1+\alpha} e^{-\frac{m}{\tau_i}}, \tag{14}$$

with q_N a normalization factor. The sum in Eq. (14), as a weighted infinite sum of exponentials, leads to the approximate power-law form of the $C_p^{(c)}$.

V. CONCLUDING REMARKS

We have introduced localized finite-time correlation functions as a suitable tool to explore the evolution of dynamical systems with mixed phase space. These correlation functions are sensitive to local phase space structures, quantifying the impact of stickiness due to phase-space traps on the emergence of correlations in an ensemble of chaotic trajectories. Using as a prototype model of the standard map we calculated these localized finite-time auto- and cross-correlation functions focusing on values of the nonlinearity parameter k in the regime of the local-to-global chaos transition. There the phase space is dynamically divided into three zones and the form of the aforementioned correlation functions differs in each zone. Specifically, in zone 1 (which includes the first-order unstable fixed point) the autocorrelations show an exponentially decaying trend for a range of k values around the critical $k_c \approx 0.971635...$, while the cross correlations develop power-law tails signaling their long-range character. Around the transition point the dynamics of the standard map attains intermittent characteristics that can be revealed after a suitable symbolic dynamics is introduced. The pathway from this intermittent dynamics to the emergence of long-range cross correlation is similar to the one introduced recently in Ref. [28] for 1D dissipative maps of Pomeau-Manneville type. Our results demonstrate that intermittency can effectively appear as a synergy of complicated phase-space networks involving overlaps of unstable and stable manifolds of fixed points as well as partial confinement due to remnants of destroyed invariant spanning curves. Such a network may in general be established in a low-dimensional dynamical system close to the critical point associated with the transition from local to global chaos. Furthermore it is confirmed that strong intermittency (even as effective dynamics) can generate long-range cross correlations between chaotic trajectories as an ensemble property. This scenario can be easily transferred to the emergence of long-range cross correlations between noninteracting particles as explained also in Ref. [28] and may provide a useful manipulation tool for inducing collective behavior in noninteracting systems.

ACKNOWLEDGMENTS

We thank A. K. Karlis and B. Liebchen for fruitful and illuminating discussions.

[1] H. G. Schuster and W. Just, *Deterministic Chaos: An Introduction* (Wiley-VCH, Weinheim, 2005); E. Ott, *Chaos in Dynamical Systems* (Cambridge University Press, Cambridge, 2002).

[2] G. M. Zaslavsky, Physica D **168**, 292 (2002).

[3] C. Karney, Physica D **8**, 360 (1983); J. Hanson, J. Cary, and J. Meiss, J. Stat. Phys. **39**, 327 (1985); J. Meiss and E. Ott, Physica D **20**, 387 (1986); L. Kuznetsov and G. M. Zaslavsky, Phys. Rev. E **66**, 046212 (2002).

[4] G. M. Zaslavsky, Chaos **5**, 653 (1995).
[5] T. Okushima, Phys. Rev. Lett. **91**, 254101 (2003).
[6] S. Dawson, C. Grebogi, T. Sauer, and J. A. Yorke, Phys. Rev. Lett. **73**, 1927 (1994).
[7] J. D. Szezech Jr. *et al.*, Phys. Lett. A **377**, 452 (2013).
[8] J. D. Szezech Jr., S. R. Lopes, and R. L. Viana, Phys. Lett. A **335**, 394 (2005).
[9] B. V. Chirikov, Phys. Rep. **52**, 264 (1979).
[10] A. J. Lichtenberg and M. A. Lieberman, *Regular and Chaotic Dynamics*, Applied Mathematical Sciences, Vol. 38 (Springer-Verlag, New York, 1992).
[11] J. D. Meiss, Rev. Mod. Phys. **64**, 795 (1992).
[12] S. Aubry, Physica D **7**, 240 (1983).
[13] A. B. Rechester and R. B. White, Phys. Rev. Lett. **44**, 1586 (1980); A. B. Rechester, M. N. Rosenbluth, and R. B. White, Phys. Rev. A **23**, 2664 (1981); G. M. Zaslavsky, *Physics of Chaos in Hamiltonian Systems* (Imperial College Press, London, 1998); P. Leboeuf, Physica D **116**, 8 (1998).
[14] Y. H. Ichikawa, T. Kamimura, and T. Hatori, Physica D **29**, 247 (1987); R. Ishizaki, T. Horita, T. Kobayashi, and H. Mori, Prog. Theor. Phys. **85**, 1013 (1991); Rom-Kedar and G. M. Zaslavsky, Chaos **9**, 697 (1999).
[15] F. Christiansen and A. Politi, Phys. Rev. E **51**, R3811 (1995); K. A. Mitchell, Physica D **241**, 1718 (2012).
[16] C. Grebogi and A. N. Kaufman, Phys. Rev. A **24**, 2829 (1981).
[17] J. D. Crawford and J. R. Cary, Physica D **6**, 223 (1983).
[18] J. D. Meiss *et al.*, Physica D **6**, 375 (1983).
[19] J. D. Meiss, Physica D **74**, 254 (1994).
[20] A. Adrover and M. Giona, Physica A **253**, 143 (1998).
[21] O. Barash and I. Dana, Phys. Rev. E **71**, 036222 (2005).
[22] E. G. Altmann, A. E. Motter, and H. Kantz, Phys. Rev. E **73**, 026207 (2006).
[23] J. D. Szezech *et al.*, Chaos **19**, 043108 (2009).
[24] G. Contopoulos and M. Harsoula, Int. J. Bif. Chaos **20**, 2005 (2010).
[25] O. Alus, S. Fishman, and J. D. Meiss, Phys. Rev. E **90**, 062923 (2014).
[26] V. Robins, Ph.D. Thesis, University of Colorado at Boulder, Boulder, USA, 2000.
[27] G. Schmidt, Phys. Rev. A **22**, 2849 (1980).
[28] F. K. Diakonos, A. K. Karlis, and P. Schmelcher, Europhys. Lett. **105**, 26004 (2014).
[29] J. M. Greene, R. S. Mackay, and J. Stark, Physica D **21**, 267 (1986).
[30] P. Manneville and Y. Pomeau, Phys. Lett. A **75**, 1 (1979); Commun. Math. Phys. **74**, 189 (1980); J. E. Hirsch, B. A. Huberman, and D. J. Scalapino, Phys. Rev. A **25**, 519 (1982).
[31] P. Schmelcher and F. K. Diakonos, Phys. Rev. Lett. **78**, 4733 (1997).